DOI: 10.2514/6.2024-0997

Extreme Temperature Additively Manufactured GRX-810 Alloy Development and Hot-fire Testing for Liquid Rocket Engines

Paul R. Gradl[1], Darren Tinker[2], Benjamin Williams[3]
NASA Marshall Space Flight Center, Huntsville, AL 35812

Timothy M. Smith[4], *Christopher Kantzos*[5]
NASA Glenn Research Center, Cleveland, OH 44135

Additive manufacturing (AM) has revolutionized component design for liquid rocket engines by offering rapid manufacturing capabilities. This has led to significant opportunities for development and flight programs in the propulsion industry, resulting in cost and schedule savings, as well as performance improvements through new designs and alloy development. A noteworthy example is the GRX-810 oxide dispersion strengthened (ODS) alloy, which was specifically developed for extreme temperatures. This Ni-Co-Cr based alloy was created using integrated computational materials engineering (ICME) techniques to focus on a new class of materials with exceptional temperature and oxidation-resistant properties. The GRX-810 alloy utilizes AM processes to incorporate nano-scale yttria particles throughout its microstructure, resulting in remarkable enhancements. Compared to traditional Nickel-based superalloys, the GRX-810 alloy offers a two-fold increase in tensile strength, 1,000-fold better creep properties, and two-fold improvement in oxidation resistance. NASA successfully demonstrated the development and manufacturing of components using the GRX-810 alloy through laser powder bed fusion (L-PBF) and laser powder directed energy deposition (LP-DED) processes. Extensive efforts were made to model, evaluate metallurgical properties, develop heat treatment processes, characterize the microstructure, and determine mechanical properties. The GRX-810 alloy was specifically designed for aerospace applications, including liquid rocket engine injectors, preburners, turbines, and hot-section components, capable of withstanding temperatures up to 1,100 °C. The objective of this alloy development is to bridge the temperature gap between traditional Nickel-based superalloys and refractory alloys. This paper provides a comprehensive comparison of the GRX-810 alloy with other aerospace alloys, discussing its microstructure, mechanical properties, processing advancements, component development, and hot-fire testing results. The ultimate goal of this development was to elevate the Technology Readiness Level (TRL) of the GRX-810 alloy, enabling its integration into NASA and commercial aerospace applications.

Nomenclature

AM	=	Additive Manufacturing
CMC	=	Ceramic Matrix Composites
DED	=	Directed Energy Deposition
GRX-810	=	Glenn Research Center eXtreme temperature alloy (Ni-Co-Cr ODS)

[1] Principal Engineer, Engine Systems Component Technology Branch, Associate Fellow, AIAA
[2] Combustion Devices Engineer, Engine Systems Component Technology Branch
[3] Combustion Devices Engineer, Engine Systems Component Technology Branch
[4] Materials Research Engineer, High Temperature and Smart Alloys Branch
[5] Materials Research Engineer, High Temperature and Smart Alloys Branch

DOI: 10.2514/6.2024-0997

HIP	=	Hot Isostatic Pressing
ICME	=	Integrated Computational Materials Engineering
LCH4	=	Liquid Methane
LH2	=	Liquid Hydrogen
LOX	=	Liquid Oxygen
L-PBF	=	Laser Powder Bed Fusion
LP-DED	=	Laser Powder Directed Energy Deposition
NDE	=	Non-Destructive Evaluation
ODS	=	Oxide Dispersion Strengthening
PBF	=	Powder Bed Fusion
RDRE	=	Rotating Detonation Rocket Engine
TRL	=	Technology Readiness Level

I. Introduction and Alloy Comparisons

Components on liquid rocket engines, such as combustion chambers, nozzles, injectors, gas generators, preburners, and turbine static and rotating components, operate in highly challenging environments [1]. These environments impose demands on functional design, materials, and fabrication processes, which are critical for the overall performance of the rocket engine system. While each component serves a different purpose, they share many common requirements. They must withstand the extreme conditions of high-pressure propellants, high-temperature gases, high thermal gradients, and high duty cycles all while maintaining structural integrity with appropriate safety margins. Additionally, these components need to be lightweight to meet the requirements of the engine system and launch vehicle. Furthermore, many of these components feature intricate internal structures, including flow passages, orifices, small restrictions, and complex curvatures, to fulfill their design objectives. To achieve these design requirements, thin-walled configurations and combinations of resilient metal alloys are often employed. These components must endure these demanding operational environments for multiple reuses, necessitating robust and durable materials and manufacturing processes that are both repeatable and reproducible [2].

The selection of materials plays a critical role in the success of aerospace applications, ensuring both component and mission accomplishments. Aerospace propulsion components face unique challenges due to the demanding operational environments and the need to satisfy programmatic and system requirements, including mass considerations, economic factors, and acceptable risk levels [3]. The appropriate selection and utilization of metal alloys, along with their processing throughout the component life cycle, significantly influence the performance of these components when deployed. In these applications, materials must be carefully chosen to resist oxidation, creep, extreme temperatures, propellant compatibility, hydrogen embrittlement, hydrocarbon coking, high pressures, high thermal gradients, low- and high-cycle fatigue, as well as high-static and -dynamic loads prevalent in such harsh environments. As integral parts of the overall system, these components must consistently demonstrate performance and meet various requirements encompassing geometric aspects, physical and mechanical properties, thermophysical characteristics, and manufacturability [3]. To meet these multifaceted requirements, the ideal material must exhibit high strength, high ductility, corrosion resistance, high-fracture toughness, and often high conductivity. Such attributes enable the material to fulfill its intended purpose effectively.

Figure 1 provides an overview of different alloy classes and their respective usable temperature and stress regimes. The most often used family of alloys used for high temperature environments includes nickel-, iron-nickel, and cobalt-based superalloys. These include alloys such as Alloy 625 (Inconel 625), Alloy 718 (Inconel 718), Co-Cr, Haynes 282, and Haynes 230, among several others [4]. Many of these alloys can typically operate at temperatures in excess of 650°C for sustained durations and some in excess of 70% of their absolute melting temperature up to 1200°C for short durations or reduced life [5]. These superalloys have been used in aerospace and propulsion applications for many decades and have a lot of flight heritage. However, there are many limitations to superalloys. Creep, thermos-mechanical fatigue, corrosion, and surface erosion are common failures observed in service [6]. Age-hardenable superalloys are also susceptible to artificial aging when exposed to extended life durations and properties can vary during the lifecycle. The operating temperatures are often in the same ranges as the aging temperatures of these alloys and thus can limit the maximum service temperatures.

DOI: 10.2514/6.2024-0997

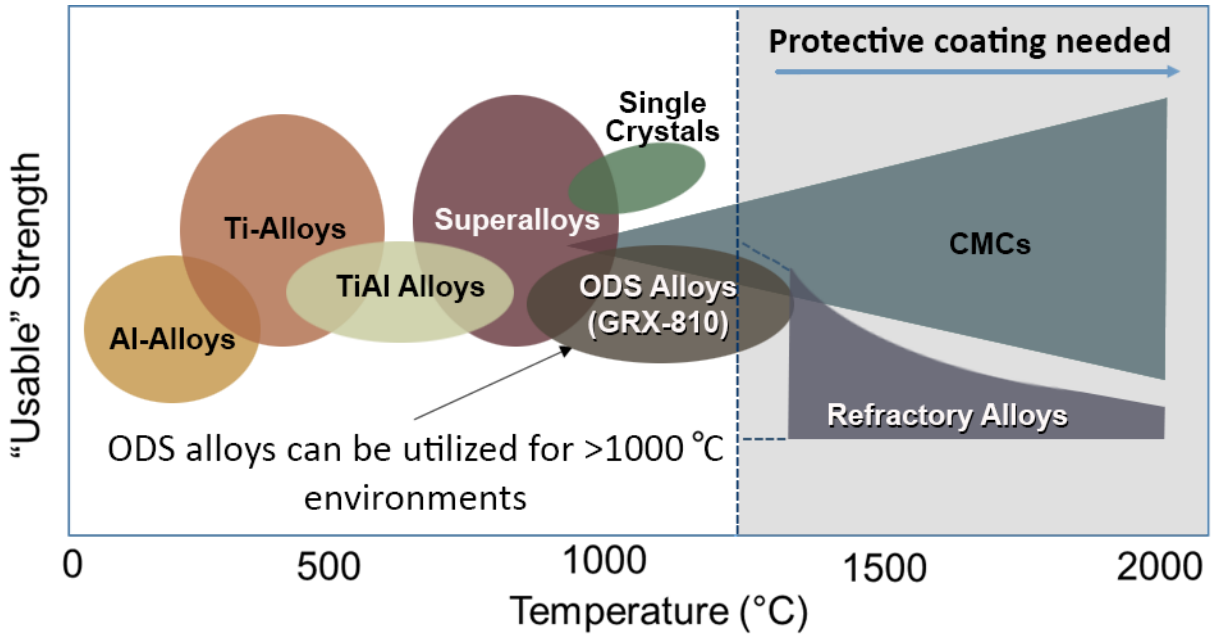

Figure 1. Comparison of maximum use temperature of aerospace alloys with GRX-810.

Inconel 718 and Inconel 625 are some of the most widely adopted materials using additive manufacturing (AM) processes such as powder bed fusion (PBF) and directed energy deposition (DED). This demand is driven by well-established literature, parameter and process maturity from AM machine manufacturers, established heat treatments, and availability of material properties [7]. While these alloys are used for a wide variety of applications, they are not ideal for all applications, yet are often used based on availability or convenience. Aluminum, titanium, and titanium-aluminide alloys have limited use applications for high temperature components. Additionally, Titanium is not used in propulsion applications requiring hydrogen as a fuel due to hydrogen environment embrittlement [8].

Ceramic matrix composites (CMC), including carbon-carbon (C-C) and carbon/silicon-carbide (C-SiC), are ultra-high temperature materials with the potential use up to (or above) 2343°C [9]. Several types of CMC's have been in developing and in use for rocket engine nozzle extensions for weight reduction and carbon-fiber composite fan blades for aviation engines. The ultra-high use temperatures are attractive, but require the use of silicon-carbide, refractory-based, inhibitor, or sealants as anti-oxidation coatings. The CMC processing also requires specialized tooling, high temperature carbonization furnaces, and coating systems that are not fully accessible across the aerospace industry.

Refractory metals like Niobium (Nb), Molybdenum (Mo), Tantalum (Ta), Rhenium (Re), and Tungsten (W) and their alloys are crucial for extreme high-temperature environments. They offer high melt temperatures, the ability to retain strength at elevated temperatures, and higher densities than Ni-base superalloys (except for Nb). Refractory metals extend the operating temperature range from 1100 to 2500 °C, depending on the material. Traditional refractory metal manufacturing is expensive due to high material costs, specialized powder production, and unique machining and joining methods. AM addresses these cost issues through reduction in buy-to-fly material usage, though AM-refractory metal components may exhibit reduced mechanical properties [10]. This can be attributed to both AM-induced micro-cracking and grain growth at elevated temperatures. Choosing a specific refractory metal or alloy depends on operating conditions like temperature, environment, stresses, and neutron fluence. Challenges in manufacturing refractory components include high ductile-to-brittle transition temperatures, ultra-high-temperature heat treatments, specialized oxidation coatings, and non-destructive evaluation (NDE) requirements [11].

Propulsion component applications are continuously being pushed for higher performance, which requires new more complex designs and new materials. New alloys being designed for these applications must meet a host of requirements. Complex designs require novel manufacturing methods, such as AM, to fulfill the internal passages and geometry requirements. This means the material must be readily printable using processes like PBF and DED. New

DOI: 10.2514/6.2024-0997

alloy development must meet programmatic and economic requirements and be both affordable and accessible. NASA has been investigating new alloys to meet the various technical and programmatic requirements including the use of oxide dispersion strengthening (ODS).

As indicated on Figure 1, between superalloys and refractory (Nb, Mo, W, etc.) alloys is this novel class of materials known as ODS alloys. These can operate in temperatures that polycrystalline Ni-base superalloys are usually inadequate. Currently, no known AM alloy has been designed for sustained use temperatures between 900-1200°C. As such, the **G**lenn **R**esearch Center e**X**treme temperature alloy (GRX-810) was designed to handle this specific regime. GRX-810 is a solid solution Ni-Co-Cr base alloy strengthened by nano-scale yttria particles to be competitive with Ni-base single crystals with up to 70% gamma prime volume fractions, but not necessarily replace [11]. Instead, GRX-810 could replace wrought alloys such as Inconel 625, Haynes 230, and Inconel 718 or Nb-base alloys such as C-103 in extreme environment applications. GRX-810 was designed for higher strength at temperatures above 810°C compared to more traditional Ni-based superalloys.

There are many targeted applications for the GRX-810 alloy. Modern advances in rotating detonation rocket engines (RDRE) and high pressure staged combustion engines are increasing heat fluxes to higher levels compared to heritage engines [12,13]. These include propulsion components such as liquid rocket engine injectors to allow for higher operating temperatures and reduce faceplate erosion. Rotating components such as turbines, blisks, and other hot section turbomachinery components could benefit from the reduced creep resistance and stress rupture at higher operating temperatures. Other high temperature components such as heat exchangers (i.e., regeneratively-cooled nozzles), control surfaces, and hot sections could also benefit from increased operating temperature alloys. GRX-810 has the potential to provide sustained lifecycles at higher operating temperatures and potentially reduce the mean time between maintenance operations. Other benefits include the simplification of heat treatments, allowing use in the as-built condition or improved properties in the hot isostatic pressing (HIP) condition.

This paper provides an overview of the GRX-810 alloy for use in these extreme environment applications. An introduction of the microstructure, characterization, and material properties are provided. A comparison to other traditional Ni-based superalloys will be presented to showcase the advantage and disadvantages. Various examples of demonstration and hot-fire test units are provided, including a summary of liquid oxygen (LOX)/liquid hydrogen (LH2) and LOX/liquid methane (LCH4) hot-fire testing. This paper demonstrates the continued maturation of the GRX-810 alloy into component applications and goal to commercialize this alloy.

II. Overview of GRX-810

The GRX-810 alloy was developed and is undergoing further refinement to increase operating temperatures and duty cycles for various propulsion components. This Ni-Co-Cr-based alloy incorporates an ODS coating, achieved economically through AM. This innovative approach addresses the historical cost challenges associated with traditional ODS alloy production. The alloy has demonstrated nearly double the tensile strength at elevated temperatures (1093 °C) compared to traditional Ni-based superalloys like Alloy 625 and Alloy 718 [11]. Additionally, the AM-produced Ni-Co-Cr alloy exhibits remarkable ductility and strain hardening, comparable to its wrought counterparts.

A coating process for the AM powder feedstock has been refined to enhance the high-temperature properties of GRX-810, resulting in ODS with a well-distributed and stabilized microstructure at elevated temperatures. The production of ODS GRX-810 components involves coating pre-alloyed base powder with <1 wt.% Y2O3 nanoparticles, ensuring even dispersion when built using laser powder bed fusion (L-PBF).

An integrated computational materials engineering (ICME) approach used to develop the GRX-810 alloy by iterating thermodynamic and density functional theory (DFT) models to predict an optimal chemistry. This chemistry was simulated through thermally cycling from room temperature up to its melting temperature without precipitating detrimental phases or compromising its grain structure. This was achieved by alloying the base Ni-Co-Cr equiatomic composition with both refractories (W, Re, and Nb) and strengthening elements such as (Ti, Al, and C). The thermodynamic models predicted B, Mo, Zr, Hf, and Ta as elements to avoid for phase stability or printability reasons. W, Re, and Al were included to increase solid solution strengthening while Nb, Ti, and C were added to precipitate

DOI: 10.2514/6.2024-0997

out stable MC carbides along grain boundaries [14]. The addition of the carbides and nano-scale oxide particles ensured a stable grain structure up to temperatures near the alloys melting point [15].

To fabricate hot-fire components with GRX-810, the material required larger quantity feedstock production, scalability, and analysis. Mechanical and microstructural tests were performed on scaled-up GRX-810 material produced using a new lot (Lot 2) of atomized feedstock from Praxair and printed on an EOS M280. Similarly, to Lot 1 (original) GRX-810, this new feedstock was coated with sub 100nm Y_2O_3 particles using the resonant acoustic mixing process [16]. Lot 2 GRX-810 builds on the EOS M280 achieved the best densities with laser energy densities between of 70-90 J/mm^3. Scanning electron images performed using a Tescan MAIA3 in the ultra-high resolution (UHR) configuration at 20kV were employed to compare the oxide dispersion between the "scaled-up" Lot 2 GRX-810 vs the original Lot 1 M100 builds as described in previous studies [14][17]. Figure 2 compares the micrographs between the two GRX-810 lots.

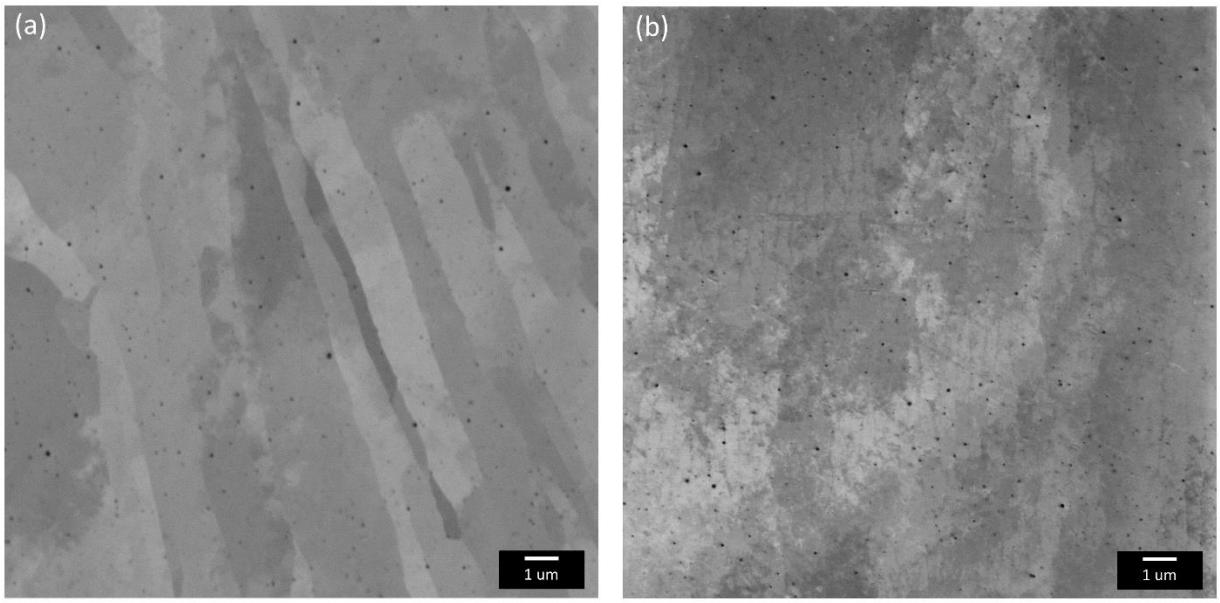

Figure 2: Secondary electron SEM micrographs of (a) Lot 1 GRX-810 produced using an EOS M100 and (b) Lot 2 GRX-810 produced using an EOS M280. The fine circular dark features are nano-scale Y2O3 particles.

The SEM micrographs in Figure 2 reveals that there does not appear to be significant differences in oxide particle size or area fraction between the two different GRX-810 lots. In fact, there appears to be a slightly higher frequency of oxides nanoparticles in the Lot 2 builds compared to Lot 1. Another interesting observation is the presence of a cellular structure, commonly observed in AM superalloys in the M280 builds [18][19]. This feature was not observed in the Lot 1 GRX-810 builds, though it is not clear if this is an effect from sample preparation between the two samples. Figure 3 reveals the grain structures between these two GRX-810 materials.

DOI: 10.2514/6.2024-0997

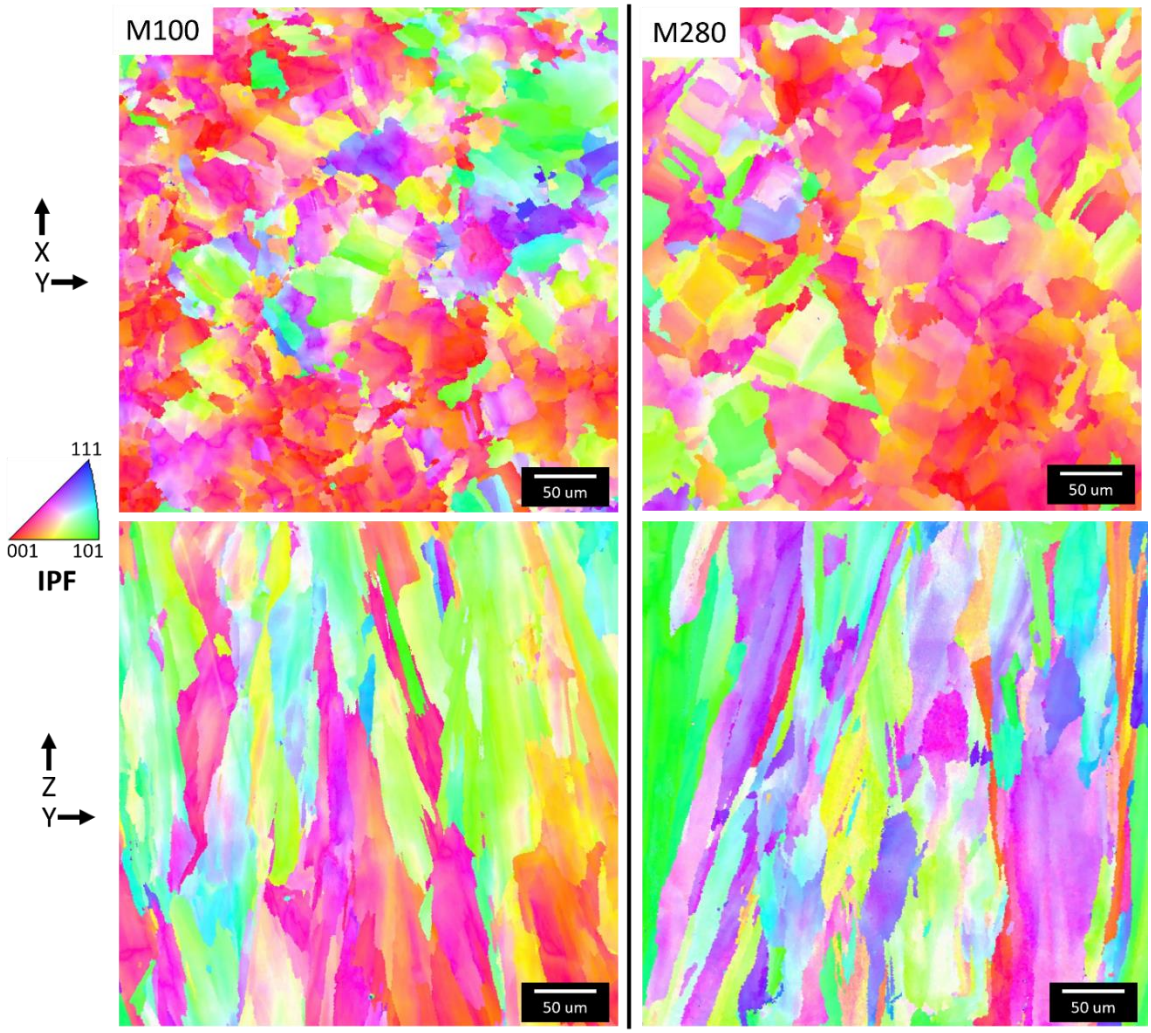

Figure 3. Electron backscatter diffraction grain orientation maps of as-built Lot 1 GRX-810 produced using an EOS M100 and Lot 2 GRX-810 produced using an EOS M280. The top maps correspond to the XY plane and the bottom maps represent the ZY plane where Z is the build direction.

The grain structure and orientation between as-built Lot 1 and Lot 2 GRX-810 builds is surprisingly similar considering the significant difference in laser build parameters that are employed between the two different AM machines (Figure 3). The M280 GRX-810 samples did reveal larger grain sizes especially in the XY-plane where the average grain diameter in the M100 sample was 39 µm compared to 59 µm in the M280 sample. Both samples exhibited prominent <001> oriented texture along the build axis and columnar grain structures. Again, both common features of AM. Neither sample recrystallized after a HIP step and each orientation map sufficiently represent the grain structure of HIPed GRX-180 as well. From Figures 2 and 3, no major microstructural difference was observed between the two GRX-810 builds.

Mechanical testing for this study was performed at Metcut Research Inc. and NASA Glenn Research Center. Tensile tests were performed at room temperature, 427°C, 650°C, 871°C at .127mm/min for the first 1.5% strain then it was increased to 1.016mm/s until failure in accordance with the ASTM E8/E21 standard, and at 1,093 °C with a constant strain rate of 1.016mm/min in accordance with the ASTM E21-17 standard. Following the tensile tests, creep tests were performed at 1,093 °C by Metcut and NASA GRC in accordance with the ASTM E139-11 standard. Testing of creep samples was continued until rupture (unless otherwise stated), after which they were then rapidly air cooled to maintain the fracture surface. All specimens were tested in Z-orientation (parallel the print direction) unless otherwise specified in the description [2]. Figure 3 compares the mechanical properties of these two lots in both the as-built condition (dashed lines) and HIPed condition (solid lines).

DOI: 10.2514/6.2024-0997

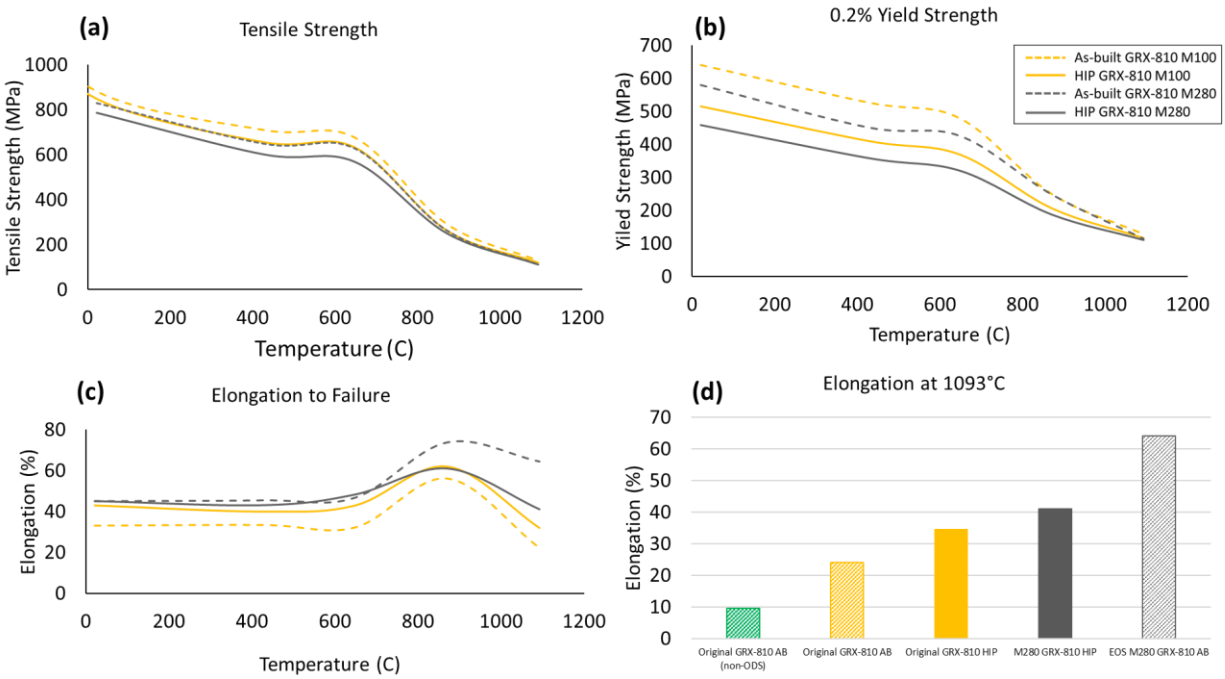

Figure 4. Tensile properties of Lot 1 GRX-810 produced using an EOS M100 and Lot 2 GRX-810 produced using an EOS M280. Notable differences in room temperature strength and high temperature elongation were observed between the different lots.

From Figure 4 a few notable differences between Lot 1 and Lot 2 GRX-810 can be observed. At lower temperatures Lot 1 GRX-810 exhibited higher tensile and yield strength (Figure 3a and 3b). This can likely be explained by Hall-Petch as the Lot 1 GRX-810 did exhibit a finer grain size [20]. This difference in tensile strength lessened as the temperature increased and both versions of GRX-810 exhibited similar strengths at 1093°C. However, the elongation (Figure 3c) of Lot 2 EOS M280 GRX-810 samples was significantly higher at 1093C compared to the original Lot 1 GRX-810. This may also be a consequence of the grain differences between the two materials. This difference in elongation may also represent an improved oxide dispersion in Lot 2 compared to Lot 1. Interestingly in NiCoCr based alloys, tensile elongation improves at elevated temperatures when nano-scale oxides are included in the microstructure [21]. This improvement is shown in Figure 3d, where non-ODS GRX-810 was found to be much less ductile at 1093°C compared to the other ODS versions. At these elevated temperatures, grain boundary oxidation begins to play a strong role in mechanical properties and the oxides are thought to help improve oxidation and stabilize grain boundaries resulting in improved ductility and tougher materials. Whether this is due to the oxides affecting the oxidation behavior itself, or simply stabilizing the microstructure is not well understood. The better oxide distribution may also be playing a role in the creep properties of Lot 2 GRX-810 as shown in Figure 5.

DOI: 10.2514/6.2024-0997

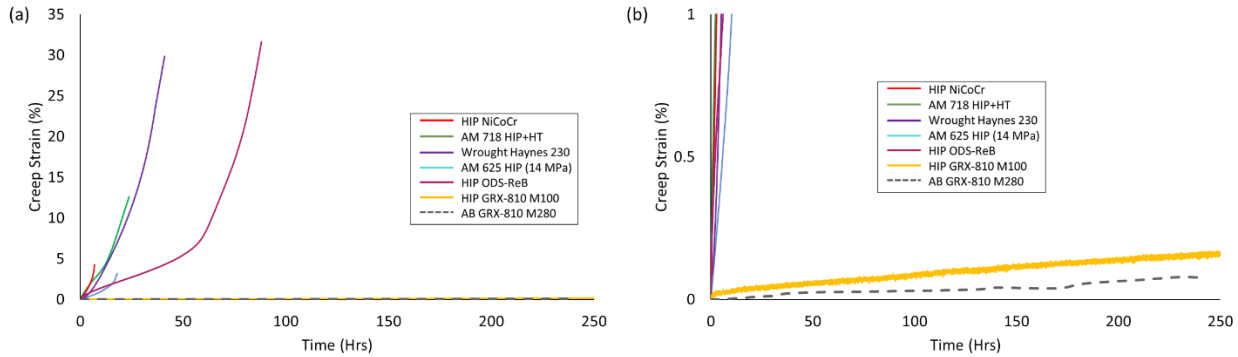

Figure 5. Creep strength of Lot 1 GRX-810 produced using an EOS M100 and Lot 2 GRX-810 produced using an EOS M280 compared to other conventional AM superalloys. Lot 2 GRX-810 is currently providing equivalent or superior creep strength compared to Lot 1 GRX-810 [14]**.**

Figure 5 compares the creep strength of Alloy 625, Alloy 718, alloy 230, AM NiCoCr, AM NiCoCr-ODS, Lot 1 HIPed GRX-810 and Lot 2 as-built GRX-810. From the graph it is apparent that the two GRX-810 samples have a significant increase in creep strength compared to the other alloys tested. Figure 4(b) shows the same creep tests as Figure 4(a) but zooms in to better show the GRX-810 creep curves. As of this publication, the M280 GRX-810 creep test is still ongoing but is currently performing the same or better than the previous GRX-810 test. This improved creep capability and high temperature ductility imply that the oxide distribution in the M280 builds is sufficient and possibly superior to samples from the M100 builds.

Thermal conductivity and coefficient of thermal expansion measurements were performed on the new Lot 1 M280 GRX-810 builds. Test results are shown in Figure 6, comparing the thermal conductivity of GRX-810 to many other Ni-base superalloys. The conductivity is comparable to other Ni-based superalloys. Notably, HIPed GRX-810 provides high thermal conductivity values between 750-1000°C. It is currently unclear what is the source for this conductivity increase though it most likely is microstructural.

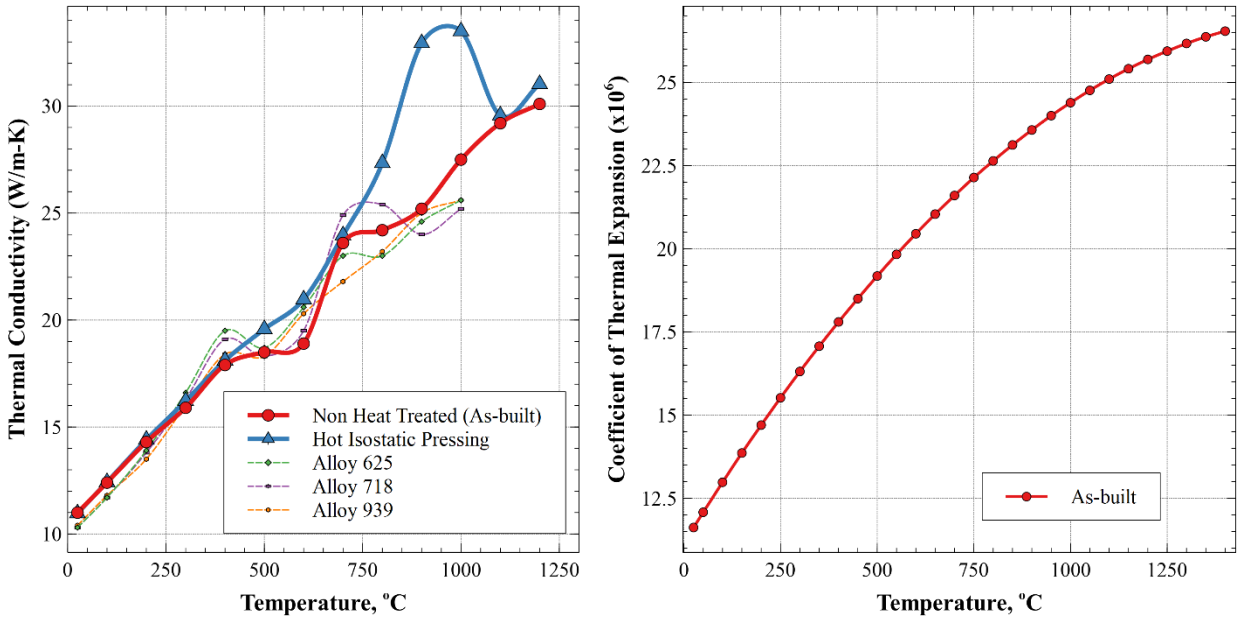

Figure 6. Thermal conductivity (left) compared to Alloy 625, 718, and 939 and CTE of Lot 2 GRX-810 produced using an EOS M280.

DOI: 10.2514/6.2024-0997

III. L-PBF Process Examples and Hardware Development

NASA prioritized early material development with the GRX-810 alloy to establish optimal process build parameters that align with the anticipated mechanical and thermophysical properties. Concurrently, emphasis was placed on component development in the initial stages of GRX-810 advancement to verify that intended complexities and geometries can be successfully built. GRX-810 is being proposed for various applications, specifically heat exchangers, turbomachinery, and components operating in high heat flux environments. In the context of liquid rocket engines, specific applications include injectors designed to mitigate the necessity for coated faceplates, regeneratively-cooled nozzles, and turbines in turbopumps. Select examples are shown in Figure 7.

Fabrication demonstrators of both non-shrouded and shrouded turbine blisks are illustrated in Figure 7A and 7E, respectively, designed to function at temperatures surpassing current limits. Figure 7B showcases an inducer aimed at demonstrating blade and internal complexity, while Figure 7F exhibits a large-scale blade featuring internal instrumentation passages. Additionally, Figure 7C presents an injector with impinging elements, and Figure 7D displays a regeneratively-cooled nozzle.

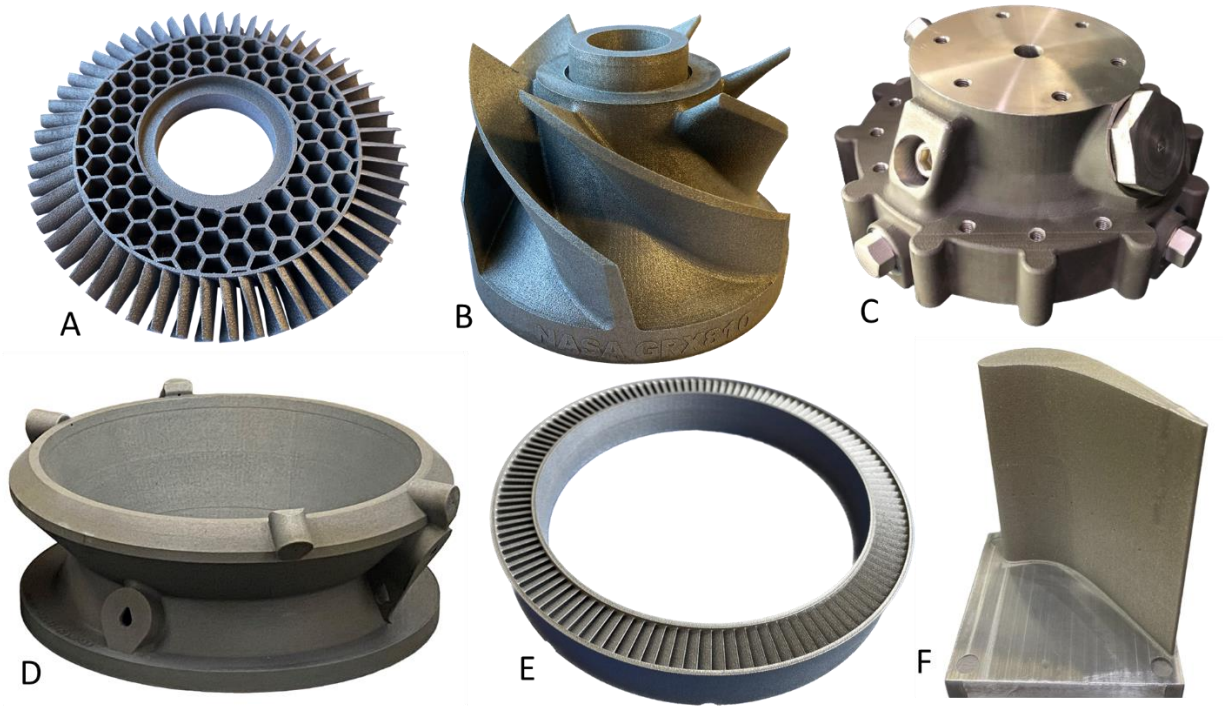

Figure 7. Various Components built using GRX-810 L-PBF: A) turbine blisk, B) inducer with internal features, C) impinging injector, D) regeneratively-cooled nozzle, E) shrouded turbine blisk, F) larger-scale turbine blade with integral instrumentation ports.

The GRX-810 alloy demonstrated comparable build speeds to typical Ni-based alloys, such as Alloy 625 and Alloy 718. Build limitations and geometries demonstrated similarities to other Ni-based alloys. Additionally, the powder exhibited consistent performance through multiple reuses during builds, maintaining uniform build geometry. Ongoing efforts continue for process development to advance the maturity of the GRX-810 alloy across various L-PBF platforms, including post-processing refinement. This entails optimizing the HIP process, as well as refining techniques like polishing, surface enhancements, and exploring other AM processes such as laser powder directed energy deposition (LP-DED).

The injector and nozzle shown in Figure 7 proceeded through the full manufacturing process flow to service in hot-fire testing. Both parts were designed for L-PBF AM with integral manifolding and channels to minimize secondary fabrication processes (i.e., welding, brazing). Limited access to nozzle manifolds required iterations for

DOI: 10.2514/6.2024-0997

powder removal (shaker table) and verification (computed tomography scanning). The most cumbersome trapped powder blocking channels was broken free through a cryogenic shock with high pressure gas flow.

Four GRX-810 injectors were L-PBF printed on the scaled-up EOS M280 with select images from the manufacturing process shown in Figure 8. Powder removal verification occurred via borescope within the manifold ports. The injector was removed from the build plate by wire electrical discharge machining (EDM) then completed HIP to obtain full density and desired fatigue properties [22]. The post-HIP image shows sacrificial stock material used to remove powder. A diagonal line is present where the EDM wire broke during build plate removal, superficially marring the final surface. After final machining, the water flow testing established flow areas and verified injector element impingement angles. The injector face was polished, followed by LOx cleaning and installation for test.

Figure 9 presents the generic manufacturing process flow with a GRX-810 alloy. The path toward service hardware parallels other L-PBF process flows for design for additive manufacturing, fabrication, and service life. The subtle difference for the GRX-810 alloy is the single heat treatment (specifically HIP) within the post-processing phase. The oxide minimizes grain growth by pinning grain boundaries throughout the L-PBF build and subsequent HIP process [11,14]. Development has also been completed to use the GRX-810 alloy in the as-built condition with some reduction to mechanical properties. The simplified post-processing can accelerate schedule by weeks, circumventing additional handling time and logistic requirements.

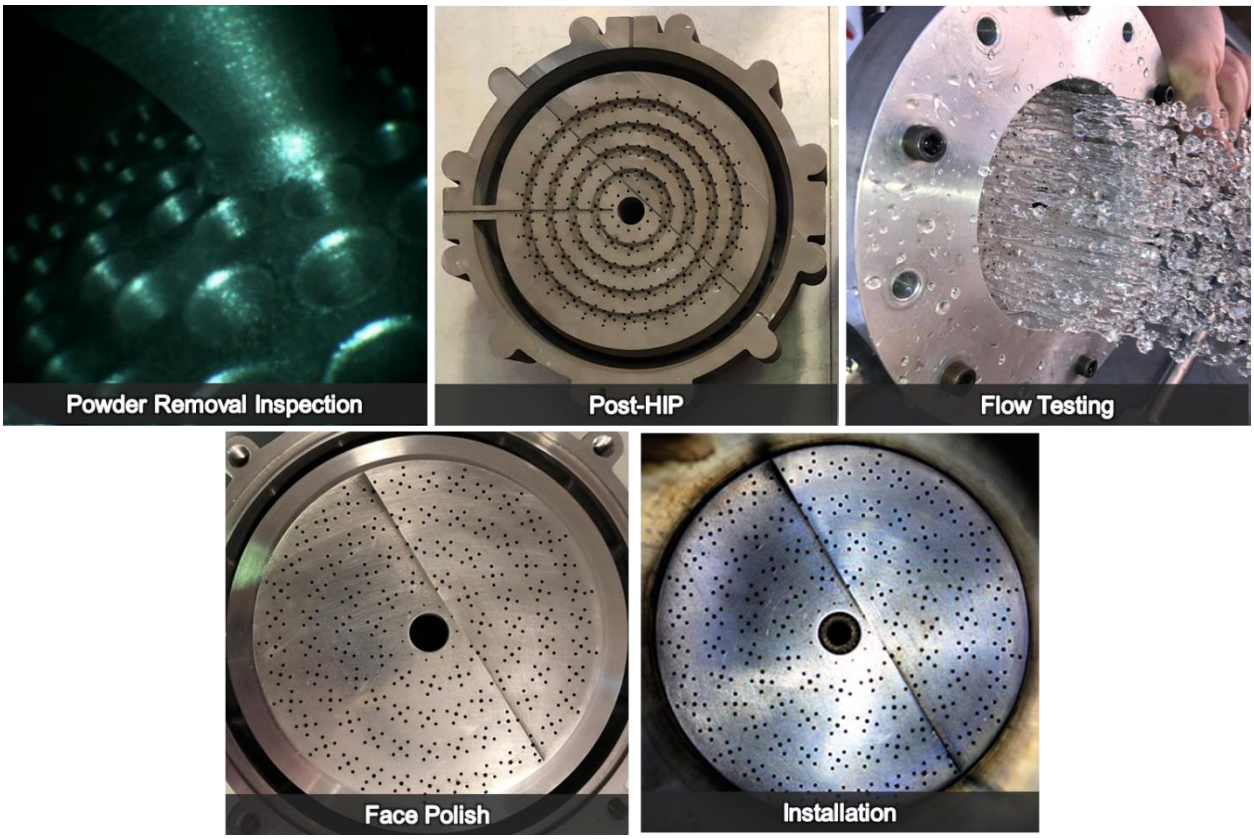

Figure 8. GRX-810 injector through selected steps of the manufacturing process flow.

DOI: 10.2514/6.2024-0997

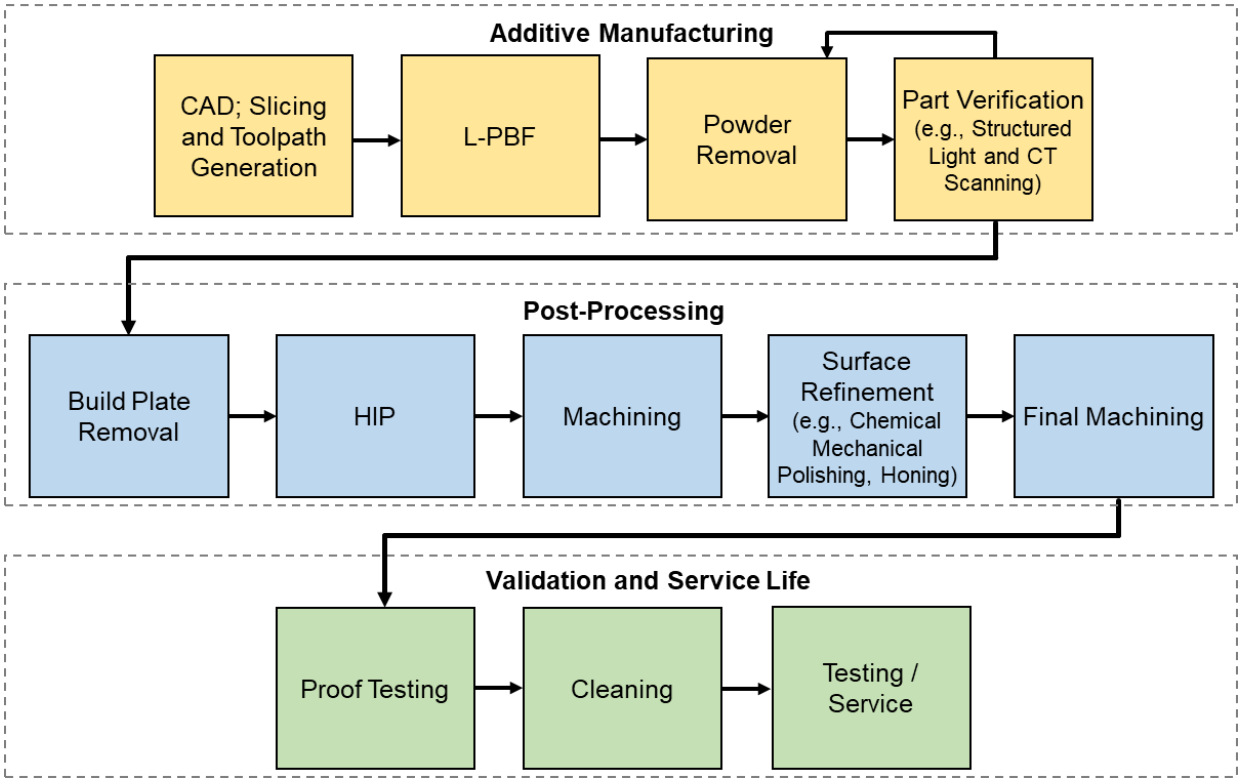

Figure 9. Generic GRX-810 L-PBF process flow.

IV. Hot-fire Testing and Results

The GRX-810 alloy technology readiness level (TRL) advanced through hot fire testing in a relevant environment. Testing was conducted at NASA MSFC test stand 115 under the Optimized and Repeatable Components using Additive (ORCA) game changing development project and Reactive Additive Manufacturing for the Fourth Industrial Revolution (RAMFIRE) collaboration. The RAMFIRE test series only incorporated the GRX-810 injector whereas the ORCA test series used both a GRX-810 injector and nozzle. Liquid oxygen/liquid hydrogen (LOX/LH2) and liquid oxygen/liquid methane (LOX/LCH4) versions of GRX-810 pentad injectors using a center mounted torch igniter were built. Two truncated ideal contour GRX-810 nozzles were fabricated as well. The injectors accumulated 3,117 seconds of hot fire across pressures of 37.4 to 57.2 bar (542 – 829 psia), shown in Table 1. The nozzles accumulated over 2,458 combined seconds.

Table 1. GRX-810 injector and nozzle hot fire summary.

Component (-)		Starts (-)	Duration (s)	Pc (bar)	Pc (psia)	MR (-)
H2 Injector	SN01	9	302.8	49.5 - 57.2	718 - 829	5.33 - 7.02
CH4 Injector	SN02	29	586.5	37.4 - 52.4	542 - 760	3.03 - 3.65
CH4 Injector	SN03	84	2,227.9	43.2 - 52.1	626 - 756	2.68 - 3.19
Nozzle	SN04	91	2,309.4	37.4 - 52.1	542 - 756	2.68 - 3.11
Nozzle	SN05	8	149.1	49.0 - 50.5	711 - 732	3.00 - 3.19

Figure 10 presents a general rendering of the thrust chamber assembly for the ORCA test series. All test assemblies used the same overall igniter assembly. All combustion chambers had the same contraction ratio and half angles with total chamber volume adjusted for a given fuel. Figure 11 shows actual thrust chamber assemblies and hot fire for both series. Fuel was used as the coolant through each nozzle and sent to a flare stack for burn-off. Throughout the ORCA test series, the fuel flow rate was reduced, raising the hot wall temperature until visual luminescence, indicating some of the potential target temperatures. The coolant flow rate was then held constant using a cavitating venturi, and

DOI: 10.2514/6.2024-0997

the chamber pressure and mixture ratio were altered to alter the nozzle heat load. The nozzle first glowed orange, then yellow as the hot wall temperature increased. Projected wall temperatures from a quasi-3D thermal model for this condition are shown in Figure 12. The model was anchored to empirical heat loads and pressure drops using the as-designed nominal geometry. The prediction assumptions and resulting temperatures are for axisymmetric and uniformly distributed coolant. It was observed this did not fully match the test conditions due to the asymmetric luminescence (c.f., Figure 11), thus more representative of a mean wall temperature.

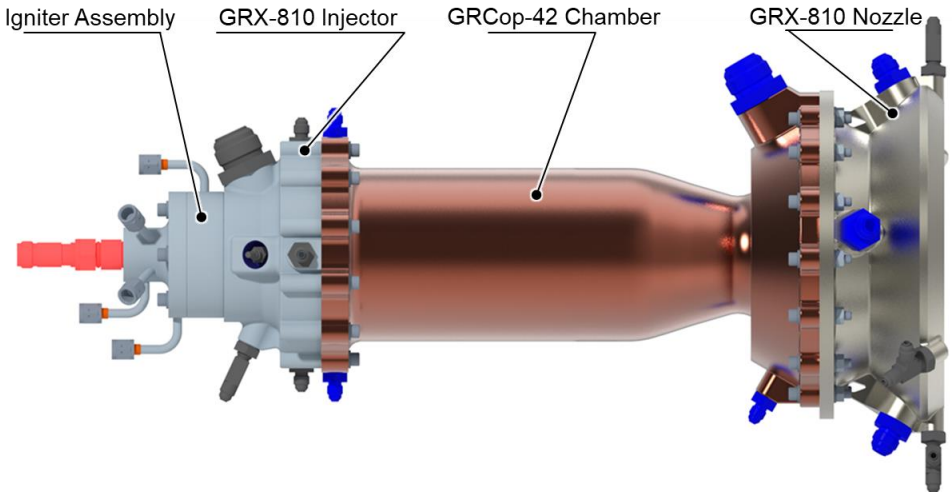

Figure 10. Thrust chamber assembly configuration for the ORCA test series.

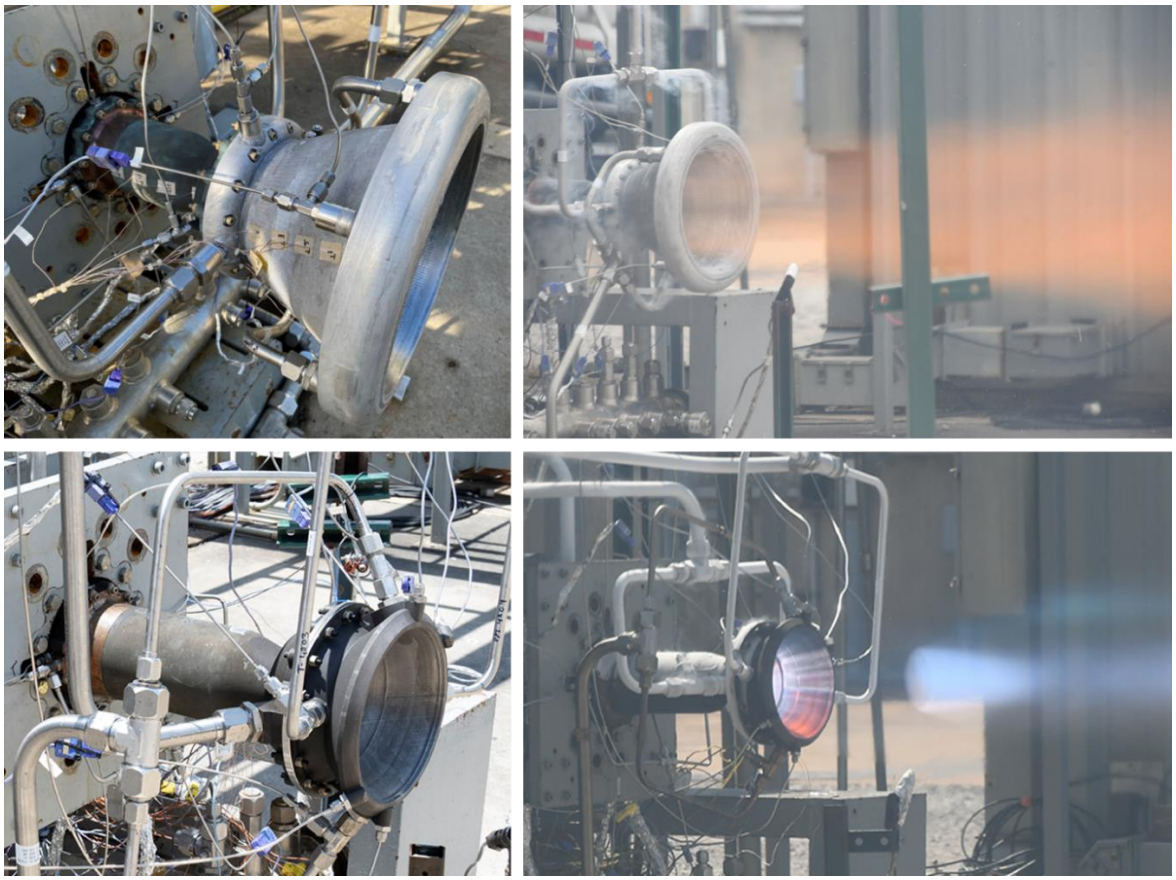

Figure 11. Hot-fire testing of GRX-810 injectors and nozzles for the RAMFIRE LOX/LH2 (top) and ORCA LOX/LCH4 (bottom) test series.

DOI: 10.2514/6.2024-0997

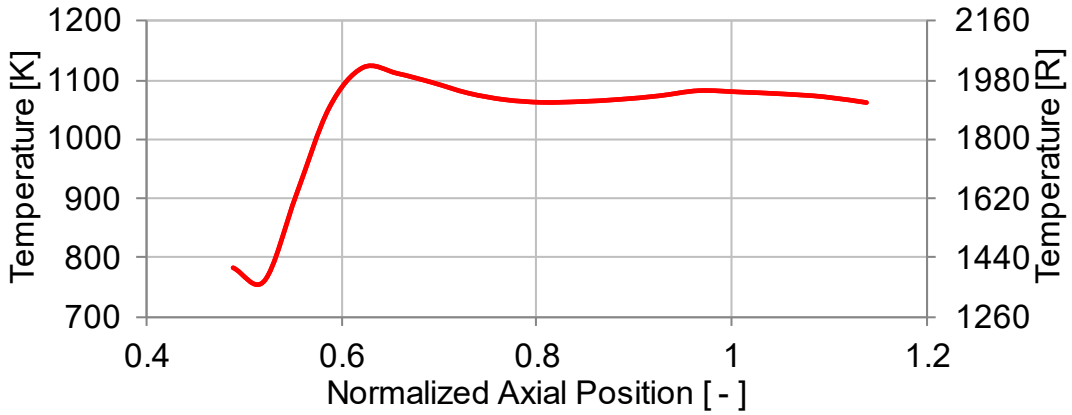

Figure 12. Nominal hot wall temperatures for the GRX-810 nozzles (LOX/LCH4).

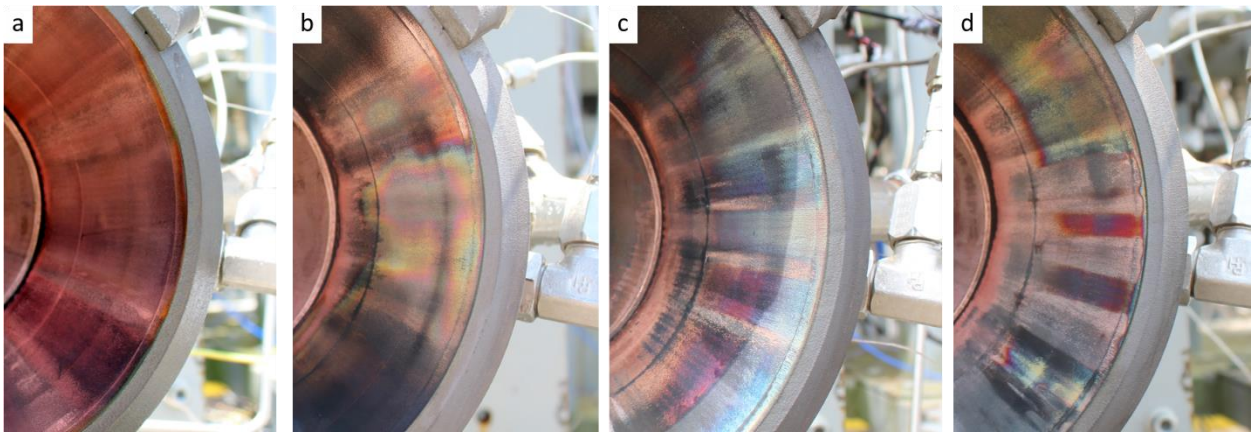

Figure 13. Progression of nozzle discoloration over (a) 15 cycles, (b) 50 cycles, (c) 67 cycles , and (d) 77 cycles.

The coolant inlet was located at forward end of the nozzle, where the combustion products impart the highest heat flux. The temperature rises rapidly due to cooling effectiveness then levels out as the heat flux decreases and the fuel increases in temperature. The nozzle was cycled 41 times over 915 seconds under these conditions, nearly half of the total test time. Bluing was apparent following luminescence and streaked with the direction of flow as shown in Figure 13 (LOX/LCH4). There were no signs of nozzle erosion throughout the test program. Surface roughness increased intermittently but correlated with locations of chamber roughening/erosion and GRCop-42 deposition on the nozzle surface. Mild bulging of the manifold was observed after segmenting the hardware but was not visually evident during test. This bulging scan be mitigated with a more robust manifold design and structural features.

The GRX-810 injector shows a noticeable improvement in robustness as compared to common superalloys such as Inconel 625 previously tested, as depicted in Figure 14. Whereas an Inconel injector experienced significant erosion after 10 LOX/LCH4 hot fire cycles, a GRX-810 injector has no evidence of damage for a near equivalent cycle count and test conditions. The only noticeable damage was scalloping of the outer row of elements on a GRX-810 injector occurring after 22 starts. Scalloping increased uniformly for this element row up through 36 starts. There was no progression of erosion for the remaining 48 starts. Mild scarfing was observed on the center of the injector near the area of the torch tube. Soot formation on the faceplate was common for mixture ratios below 2.8 and deposits were removed in-situ during higher mixture ratio conditions. Injector bluing was evident during LOX/LH2 testing as shown in Figure 15, but there were no signs of faceplate erosion

DOI: 10.2514/6.2024-0997

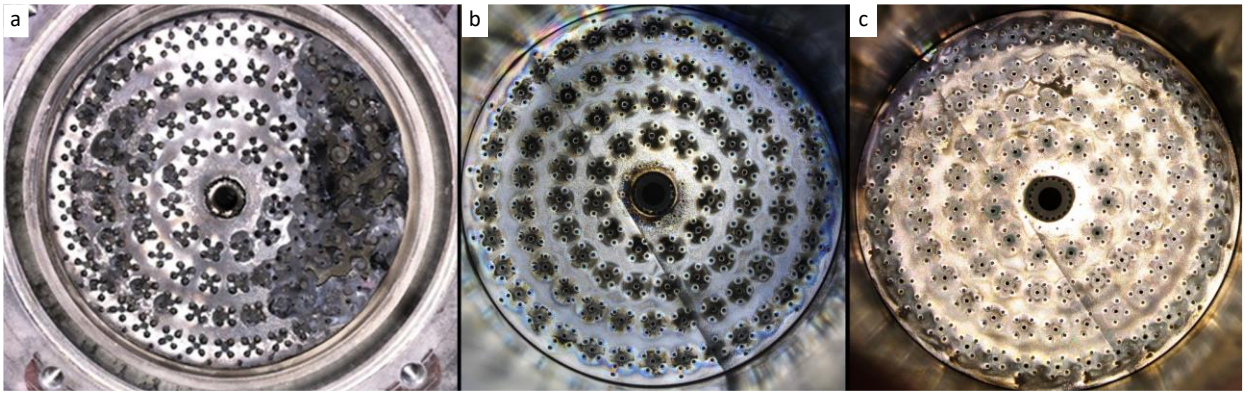

Figure 14. LOX/LCH4 hot-fire testing: (a) Inconel 625 injector following 10 tests with erosion observed, (b) GRX-810 injector following 13 tests, and (c) GRX-810 injector following 84 tests and discoloration observed.

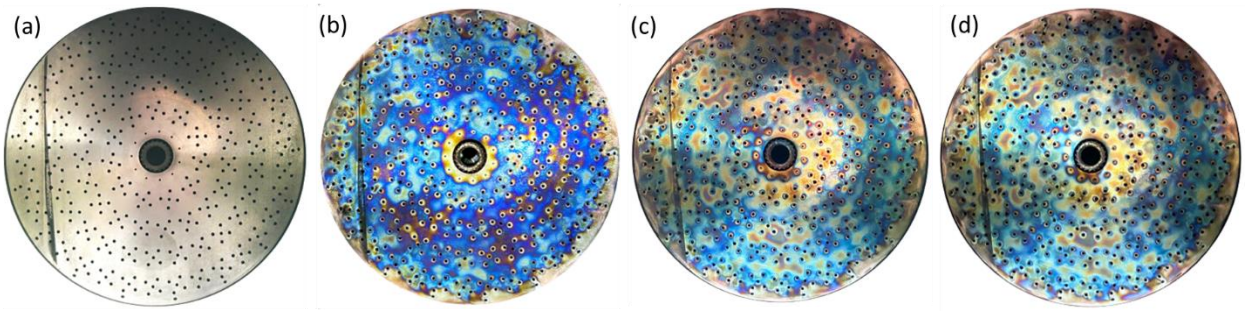

Figure 15. LOX/LH2 Hot-fire testing of GRX-810 injector. (a) Pre-test, (b) post-3 cycles, (c) post-6 cycles, (d) post-9 cycles.

V. Conclusions and Future Work

Additive manufacturing has played a transformative role in the design and fabrication of liquid rocket engine components, exemplified by the development and successful demonstration of the GRX-810 oxide dispersion strengthened (ODS) alloy. This Ni-Co-Cr based alloy, engineered using integrated computational materials engineering (ICME) techniques, showcases exceptional temperature and oxidation-resistant properties. The incorporation of nanoscale yttria particles in the powder feedstock results in remarkable enhancements – offering an improvement in tensile strength, creep properties, and oxidation resistance compared to traditional Nickel-based superalloys. The GRX-810 alloy exhibits a two-fold increase in tensile strength, 1,000-fold better creep properties, and a two-fold improvement in oxidation resistance compared to traditional Nickel-based superalloys. The alloy was demonstrated on different scale laser powder bed fusion (L-PBF) platforms and with similar properties. Additionally, the single heat treatment using hot isostatic pressing (HIP), minimizes grain growth, enhancing the material's structural integrity during AM.

The successful application of the GRX-810 alloy in hot-fire testing, particularly in liquid oxygen/liquid hydrogen (LOX/LH2) and liquid oxygen/liquid methane (LOX/LCH4) environments, demonstrates its robustness and readiness for aerospace applications. The GRX-810 technology readiness level (TRL) has advanced through hot-fire testing, accumulating 3,117 seconds of hot fire across various pressures and propellant combinations. The GRX-810 injector shows a noticeable improvement in robustness compared to common superalloys, showcasing its potential for commercial aerospace applications.

Future work involves additional scaling and analysis of the GRX-810 alloy feedstock and both L-PBF and laser powder directed energy deposition (LP-DED) builds for large-scale production and broader applications. The focus will be on the continued maturation of the GRX-810 alloy into component applications, with the final goal of

DOI: 10.2514/6.2024-0997

commercialization. Research efforts are exploring additional applications within aerospace and into the energy industry. Collaboration with industry partners is crucial for integrating the GRX-810 alloy into both NASA and commercial aerospace programs, elevating its TRL for widespread use.

Acknowledgements

The authors would like to thank the Optimized and Repeatable Components using Additive (ORCA) under STMD Game Changing Program, Transformational Tools and Technology (TTT), and SLS Liquid Engine Office (LEO) projects for their continued support. Specifically, John Fikes, John Vickers, Lynn Machamer, Johnny Heflin, Keegan Jackson, Kristin Morgan, and Dale Hopkins. There are several team members to thank including Tessa Fedotowsky, Bob Witbrodt, Adam Willis, MSFC CT Team, Tom Teasley, Matt Marsh, Colton Katsarelis, Ken Cooper (Nam Pros), Dennis Strickland, Kendall Feist, Nick Hensley, Steve Baggette, TS115 test crew, and many others involved. All trademarks are the property of their respective owners. This paper describes objective technical results and analysis. Any subjective views or opinions that might be expressed in the paper do not necessarily represent the views of the National Aeronautics and Space Administration (NASA) or the United States Government.

References

[1] P.R. Gradl, S.E. Greene, C. Protz, B. Bullard, J. Buzzell, C. Garcia, J. Wood, K. Cooper, J. Hulka, R. Osborne, Additive manufacturing of liquid rocket engine combustion devices: A summary of process developments and hot-fire testing results, in: 2018 Jt. Propuls. Conf., American Institute of Aeronautics and Astronautics Inc, AIAA, 2018. https://doi.org/10.2514/6.2018-4625.

[2] Paul R. Gradl, Omar R. Mireles, Christopher S. Protz, Chance P. Garcia, Metal Additive Manufacturing for Propulsion Applications, 1st ed., American Institute of Aeronautics and Astronautics, Inc., Reston, VA, 2022. https://doi.org/10.2514/4.106279.

[3] B.N. Bhat, ed., Aerospace Materials and Applications, American Institute of Aeronautics and Astronautics, Inc., Reston ,VA, 2018. https://doi.org/10.2514/4.104893.

[4] Matthew J. Donachie Stephen J. Donachie, Superalloys: A Technical Guide, 2nd ed., ASM International, 2002.

[5] A. Nowotnik, Nickel-Based Superalloys, Ref. Modul. Mater. Sci. Mater. Eng. (2016). https://doi.org/10.1016/B978-0-12-803581-8.02574-1.

[6] B. Swain, P. Mallick, S. Patel, R. Roshan, S.S. Mohapatra, S. Bhuyan, M. Priyadarshini, B. Behera, S. Samal, A. Behera, Failure analysis and materials development of gas turbine blades, Mater. Today Proc. 33 (2020) 5143–5146. https://doi.org/10.1016/J.MATPR.2020.02.859.

[7] P. Gradl, D. Tinker, A. Park, O. Mireles, M. Garcia, R. Wilkerson, C. Mckinney, Robust Metal Additive Manufacturing Process Selection and Development for Aerospace Components, J. Mater. Eng. Performance, Springer. (2021). https://doi.org/10.1007/s11665-022-06850-0.

[8] J. Lee, Hydrogen embrittlement, 2016. https://ntrs.nasa.gov/.

[9] P.G. Valentine, P.R. Gradl, Extreme-Temperature Carbon- and Ceramic-Matrix Composite Nozzle Extensions for Liquid Rocket Engines, Proc. Int. Astronaut. Congr. IAC. 2019-Octob (2019) 21–25.

[10] O.R. Mireles, O. Rodriguez, Y. Gao, N. Philips, Additive manufacture of refractory alloy c103 for propulsion applications, in: AIAA Propuls. Energy 2020 Forum, American Institute of Aeronautics and Astronautics Inc, AIAA, 2020: pp. 1–13. https://doi.org/10.2514/6.2020-3500.

[11] P. Gradl, O.R. Mireles, C. Katsarelis, T.M. Smith, J. Sowards, P. Chen, D. Tinker, C. Protz, T. Teasley, D.L. Ellis, C. Kantzos, Advancement of Extreme Environment Additively Manufactured Alloys for Next Generation Space Propulsion Applications, Acta Astronaut. 211 (2023) 483–497. https://doi.org/10.1016/j.actaastro.2023.06.035.

[12] T.W. Teasley, T.M. Fedotowsky, P.R. Gradl, B.L. Austin, S.D. Heister, Current State of NASA Continuously Rotating Detonation Cycle Engine Development, in: AIAA Scitech 2023, AIAA, 2023: pp. 1–24. https://doi.org/10.2514/6.2023-1873.

[13] T. Teasley, B. Williams, A. Larkey, C. Protz, P. Gradl, A Review Towards the Design Optimization of High-Performance Additively Manufactured Rotating Detonation Rocket Engine Injectors, AIAA Propuls. Energy Forum, 2021. (2021). https://doi.org/10.2514/6.2021-3655.

[14] T.M. Smith, C.A. Kantzos, N.A. Zarkevich, B.J. Harder, M. Heczko, P.R. Gradl, A.C. Thompson, M.J.

DOI: 10.2514/6.2024-0997

Mills, T.P. Gabb, J.W. Lawson, A 3D printable alloy designed for extreme environments, Nature. (2023). https://doi.org/10.1038/s41586-023-05893-0.

[15] T.M. Smith, A.C. Thompson, T.P. Gabb, C.L. Bowman, C.A. Kantzos, Efficient production of a high-performance dispersion strengthened, multi-principal element alloy, Sci. Reports 2020 101. 10 (2020) 1–9. https://doi.org/10.1038/s41598-020-66436-5.

[16] J.G. Osorio, F.J. Muzzio, Evaluation of resonant acoustic mixing performance, Powder Technol. 278 (2015) 46–56. https://doi.org/10.1016/j.powtec.2015.02.033.

[17] T.M. Smith, A.C. Thompson, T.P. Gabb, C.L. Bowman, C.A. Kantzos, Efficient production of a high-performance dispersion element alloy, Sci. Rep. (2020) 1–9. https://doi.org/10.1038/s41598-020-66436-5.

[18] Q. song Song, Y. Zhang, Y. feng Wei, X. yi Zhou, Y. fu Shen, Y. min Zhou, X. mei Feng, Microstructure and mechanical performance of ODS superalloys manufactured by selective laser melting, Opt. Laser Technol. 144 (2021) 107423. https://doi.org/10.1016/j.optlastec.2021.107423.

[19] W.M. Tucho, P. Cuvillier, A. Sjolyst-Kverneland, V. Hansen, Microstructure and hardness studies of Inconel 718 manufactured by selective laser melting before and after solution heat treatment, Mater. Sci. Eng. A. 689 (2017) 220–232. https://doi.org/10.1016/j.msea.2017.02.062.

[20] D.J. Dunstan, A.J. Bushby, Grain size dependence of the strength of metals: The Hall-Petch effect does not scale as the inverse square root of grain size, Int. J. Plast. 53 (2014) 56–65. https://doi.org/10.1016/j.ijplas.2013.07.004.

[21] J. Telesman, P. Kantzos, J. Gayda, P.J. Bonacuse, a. Prescenzi, Microstructural Variables Controlling Time-Dependent Crack Growth in a P/M Superalloy, Superalloys 2004 (Tenth Int. Symp. (2004) 215–224. https://doi.org/10.7449/2004/Superalloys_2004_215_224.

[22] NASA, NASA-STD-6030 and NASA-STD-6033 Compliance Matrix Forms, (2021).